Bijel-templated hydrogel membranes for pH-responsive water filtration

Henrik Siegel[1], *Martin F. Haase*[1*]

Correspondence: m.f.haase@uu.nl

[1] Van't Hoff Laboratory of Physical and Colloid Chemistry, Debye Institute for Nanomaterials Science, Department of Chemistry, Utrecht University, Utrecht, The Netherlands

Abstract

Hydrogels are cross-linked, hydrophilic polymer networks with growing applications in membrane filtration. However, their filtration performance is limited by fouling on the membrane surface. While nanoparticle coatings are well-known for providing anti-fouling properties, their incorporation into the hydrogel surface is hindered by nanoparticle agglomeration in many hydrogel polymers. In this work, we introduce the synthesis of hydrogel membranes with nanoparticle-decorated surfaces made from bicontinuous interfacially jammed emulsion gels (bijels) for pH-responsive water filtration. We fabricate bijel films by coating the bijel precursor onto flat-sheet substrates using roll-to-roll solvent transfer induced phase separation (R2R-STrIPS). Our study shows that the precursor wetting on the substrate and the nanoparticle surface modification with surfactant control the bijel structure and internal pore sizes. Hydrolysis converts the bijel films into polyacrylic acid hydrogels. Using confocal microscopy analysis, we reveal that the swelling of the hydrogel in response to increasing water pH leads to a closure of the membrane surface pores. Flux measurements show that the swollen hydrogel blocks water flow, while decreasing the water pH re-opens the hydrogel surface pores and enables water permeation. By the separation of emulsion droplets our bijel-hydrogel membranes showcase the potential of bijels as templates for smart microfiltration membranes for water filtration, drug delivery, and tissue engineering.

Keywords: Nanoparticles, bijels, hydrogel, phase separation, pH-responsive, separation membranes

1. Introduction

Separation membranes are important materials with applications in water treatment[1], food processing[2], chemical purification[3], and energy production[4]. Membrane-based processes have attracted growing interest for improving the energy efficiency of industrial separations compared to traditional methods such as distillation.[5] The increasing demand for separation membranes calls for membrane materials with separation functionalities tailored to the application purpose.[6] However, conventional polymer and ceramic membranes have rigid structures which require complex surface modifications to adjust their separation performance.[7,8] To facilitate control over the separation properties, research has focused on designing separation membranes with self-regulated permeability and selectivity.

To impart self-regulated separation properties, membranes can be fabricated from polymers that adapt their structure in response to the physicochemical conditions in the local environment.[9] Stimuli-responsive polymers such as polyacrylic acid (PAA), polyvinyl alcohol or poly(*N*-isopropylacrylamide) change their conformation upon variations in pH[10], temperature[11], or the exposure to light[12]. For example, the stimuli-responsive swelling of hydrogel polymer membranes allows to control the permeation of fluids[13,14], the gating of ions[15,16] and the rejection of small molecules[17]. On the downside, hydrogel membranes are susceptible to fouling caused by the deposition of colloidal matter, organic substances or biofilms.[18,19] To prevent membrane fouling, anti-fouling materials such as nanoparticles need to be incorporated into the hydrogel.[20] However, the aggregation and leaching of nanoparticles in polymer mixtures complicate the synthesis of hydrogels with uniformly distributed nanoparticles across the membrane.[21]

Recently, the fabrication of hydrogel membranes with homogeneously covered nanoparticle surfaces has been introduced using bicontinuous interfacially jammed emulsion gels (bijels).[22–26] Bijels are porous materials formed from arresting the phase separation of a mixture of oil and water with silica nanoparticles.[27,28] Unlike most hydrogels which are prepared from the phase separation of polymer solutions, bijels are formed with monomers as the oil phase which are polymerized after phase separation to solidify the hydrogel membrane.[23,29] The nanoparticle-decorated surfaces make bijel-templated hydrogels interesting functional materials for stimuli-responsive membrane separations.

In this study, we present the synthesis of bijel-templated hydrogel filtration membranes that open and close their surface pores in response to changes in the water pH. To this end, we fabricate nanoparticle-stabilized bijel films via roll-to-roll solvent transfer induced phase separation (R2R-STrIPS). We coat the bijel precursor solution onto various flat-sheet substrates and investigate the bijel precursor wetting to enable the collection of polymerized bijel films from the substrate. The porous structure of the bijel film can be controlled by changing the nanoparticle surface modification with surfactant. We hydrolyze the bijel films to obtain PAA-hydrogel membranes. Confocal microscopy analysis shows that swelling of the PAA hydrogel at alkaline pH leads to a closure of the membrane surface pores. Complementary measurements of the water permeability demonstrate that the pH-responsive pore closure enables the

regulation of water flow with bijel-templated PAA hydrogels. We perform emulsion separation experiments showing that these PAA hydrogel membrane can be used for the microfiltration of oil droplets.

2. Results and discussion

2.1 Bijel film synthesis

We synthesize bijel films in a roll-to-roll (R2R) film coating process called "R2R-STrIPS".[30] To this end, we prepare the bijel precursor by mixing the liquids *tertiary*-butyl acrylate (*t*-BA), 1,4-butanediol diacrylate (BDA) and water using ethanol as solvent at the composition specified in the ternary phase diagram in **Figure 1A** (for details see SI sections S1 and S2). In this liquid precursor mixture, we homogeneously disperse 33 wt-% silica nanoparticles (Ludox® TMA, 20 nm, acidified to pH 1.7; abbreviated as SNPs) with cetyltrimethylammonium bromide (CTA^+) as surfactant.

For R2R-STrIPS, the precursor mixture is pumped through a slit onto polyethylene terephthalate (PET) substrate submerged in water (pH 1.7; **Figure 1B-*i***). When the precursor leaves the slit and contacts the water bulk, ethanol starts to diffuse out into the surrounding water. The removal of ethanol causes the precursor mixture to undergo solvent transfer induced phase separation (STrIPS). As illustrated in **Figure 1B-*ii***, the precursor phase separation is arrested by the jamming of the CTA^+-modified SNPs at the interface formed between *t*-BA and water. We solidify the resulting bijel films by polymerizing the *t*-BA monomers with high-intensity UV-light. To cross-link *t*-BA upon polymerization, we incorporate 8 wt-% 1,4-butanediol diacrylate (BDA) in the *t*-BA monomer solution. **Figure 1C** shows a photograph of the polymerized bijel film with green fluorescence of Coumarin 6 dye embedded in poly(*t*-BA) under UV-light.

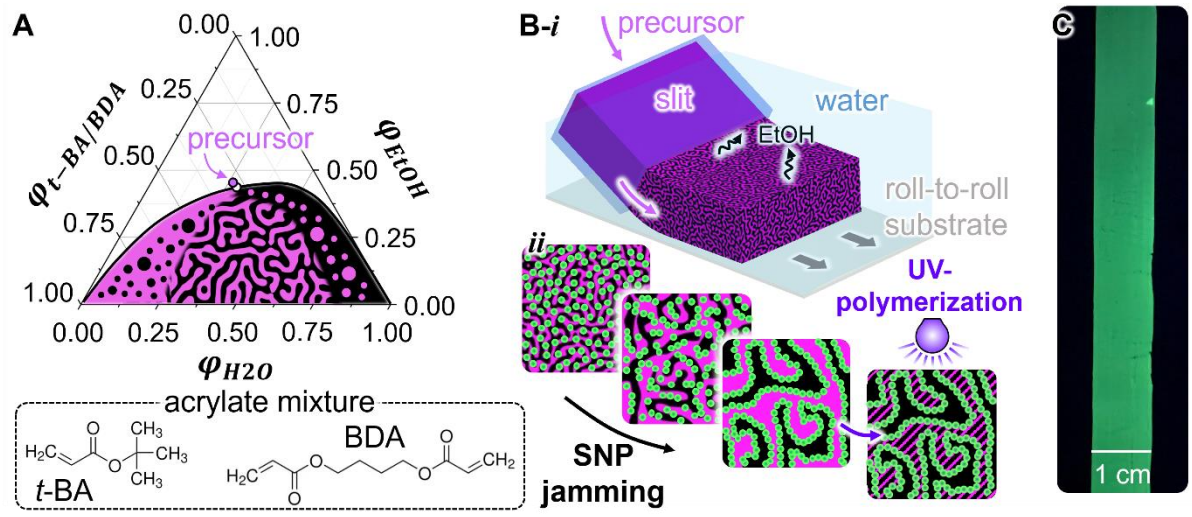

Figure 1. Bijel film fabrication *via* R2R-STrIPS. **A** Ternary liquid phase diagram of a mixture of 92 wt-% *tertiary*-butyl acrylate (*t*-BA) and 8 wt-% 1,4-butanediol diacrylate (BDA), water, and ethanol (EtOH) plotted in liquid volume fractions φ. The critical point is given as white dot with a schematic representation of the phase separation of *t*-BA (magenta) and water (black). **B-*i*** Bijel film fabrication *via* R2R-STrIPS. ***ii*** Sketches showing the nanoparticle jamming of the *t*-BA/water interface. Magenta colour represents *t*-BA, black colour water and green colour nanoparticles. **C** Fluorescent photograph of polymerized bijel film.

After R2R-STrIPS we collect the polymerized bijel film along with the PET substrate. To enable the use as hydrogel filtration material, the bijel film must be detached from the substrate. The removal of the PET, however, is hindered by the adhesion of the bijel film. Therefore, we investigate how the adhesion properties of the bijel film vary with different substrate materials.

2.2 Substrate wetting and bijel film collection

Previous research has shown that bijel films adhere to PET as the precursor mixture wets the substrate during R2R-STrIPS.[30] Since the poly(*t*-BA) bijel film also adheres to PET, we hypothesize that the detachment of the bijel from the substrate can be achieved by selecting a substrate material from which the precursor mixture de-wets. To test our hypothesis, we coat the bijel precursor onto cellulose acetate and cellulose as these substrates are more hydrophilic than PET and test the bijel adhesion and precursor wetting.

We find that R2R-STrIPS produces macroscopically uniform bijel films on all substrate materials tested. While the polymerized bijel film also adheres to cellulose acetate, the bijel film detaches from cellulose even before polymerization. To investigate why the bijel film peels off from cellulose but remains attached to PET and cellulose acetate, we analyze the bijel structure formed on the different substrates.

The bijel film structure is imaged using confocal laser scanning microscopy (CLSM). For CLSM we label the poly(*t*-BA) domains with the fluorescence dye Nile red, and the SNPs are labelled with Rhodamine 110 chloride. **Figure 2A-*i*** shows a 3D-CLSM image of the bijel film prepared on PET. The small pores formed at the bijel surface result from the fast diffusion of ethanol, facilitating interfacial SNP jamming at an early stage of the *t*-BA/water phase separation.[31] At the bottom of the bijel film, large poly(*t*-BA) clusters with distinct water pores extend across the PET substrate. We obtain a similar structure for the bijel made on cellulose acetate with larger water pores at the bottom of the film presented in **Figure 2A-*ii***.

Remarkably, the bijel film coated on cellulose (**Figure 2A-*iii***) exhibits small pores at both the top *and* bottom surface. This porous structure indicates that diffusion of ethanol also occurs through the bottom of the bijel film. As cellulose is a hydrophilic material, it can absorb water from the surrounding water bulk. The cellulose substrate can already be wetted by water when the precursor mixture is deposited. As a result, the bijel film forms on a thin layer of water above the cellulose which can explain the diffusion of ethanol out of the bijel bottom during R2R-STrIPS. Simultaneously, bijel de-wetting from the water-drenched cellulose can lead to the detachment of the bijel film from the substrate. To understand the different bijel adhesion behaviors on PET, cellulose acetate, and cellulose, we study the bijel wetting on these substrates by precursor wetting experiments and contact angle measurements.

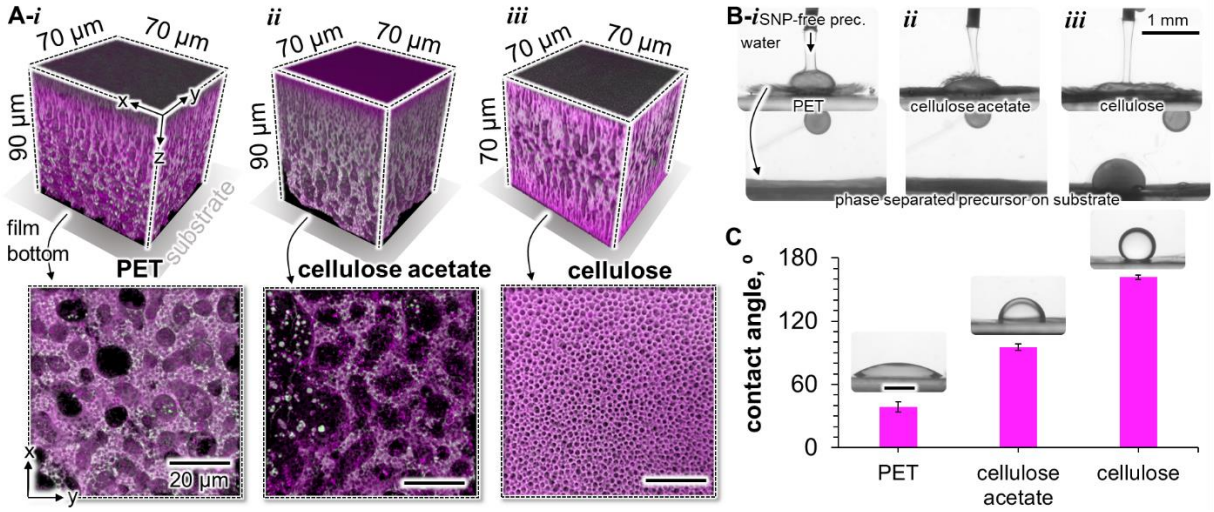

Figure 2. Substrate adhesion and wetting of bijel films. **A** 3D confocal laser scanning microscopy (CLSM) images of bijel films made on substrates ***i-iii*** with magnified projections of the film bottom below. Magenta colour represents poly(*t*-BA), black colour water and green colour SNPs. **B** Photograph of the injection of SNP-free precursor mixture (41 mM CTA^+) onto substrates ***i-iii*** in water (pH 1.7) with photograph of the phase separated precursor after injection below. **C** Contact angles of pure *t*-BA on substrates in water (pH 1.7) with photographs of sessile *t*-BA droplets. Black scale bar is 1 mm.

To test the substrate wetting, we inject SNP-free precursor mixtures containing 41 mM CTA^+ onto PET, cellulose acetate, and cellulose in water (pH 1.7). The precursor mixtures undergo phase separation upon injection, evident by the dark blur of nucleated *t*-BA droplets in water. We exclude SNPs from this experiment because interfacial SNP jamming during phase separation would prevent the spreading of liquids on the substrate materials. After phase separation of the precursor, the residual *t*-BA forms a layer on both PET and cellulose acetate captured in **Figures 2B-*i*** and ***ii***. However, on cellulose, *t*-BA balls up into a droplet (**Figures 2B-*iii***). We quantify this observation by measuring the contact angle of pure *t*-BA on these substrates in water (pH 1.7). **Figure 2C** shows that the contact angle amounts to 162° on cellulose, and decreases significantly to 95° on cellulose acetate and 39° on PET. The decreasing contact angle together with the precursor liquid spreading indicates that *t*-BA wets on PET and cellulose acetate, but de-wets on cellulose.

The *t*-BA wetting likely facilitates the adhesion of the bijel films on PET and cellulose acetate by the formation of large poly(*t*-BA) domains on these substrates. In contrast, the de-wetting of *t*-BA on cellulose can trigger the bijel detachment. After polymerization, the detached bijel films can be collected from the cellulose substrate. Employing these bijels as hydrogel filtration materials, however, requires control over the bijel film structure and permeability. In the following, we study the effect of the CTA^+ concentration on the porous bijel microstructure.

2.3 Effect of CTA^+ concentration on bijel structure

We fabricate bijel films from precursor mixtures containing different CTA^+ concentrations. By raising the concentration of CTA^+ in the bijel precursor, the adsorbed amount of CTA^+ on the SNPs increases and changes their wettability for stabilizing the interface between *t*-BA and water.[32] CLSM analysis

reveals that the CTA^+ concentration has a pronounced effect on the bijel structure. The 3D-CLSM image in **Figure 3A-*i*** shows discrete, tubular water pores for the bijel film prepared at 32 mM CTA^+. Increasing the CTA^+ concentration to 41 mM produces elongated water pores (**Figure 3A-*ii***). At 50 mM CTA^+, the water pores merge into an interwoven arrangement with poly(*t*-BA) by including discrete poly(*t*-BA) droplets inside the water-filled interior (**Figure 3A-*iii***). At 55 mM CTA^+, thinner bijel films are produced with a poly(*t*-BA)-rich shell and virtually hollow center (**Figure 3A-*iv***).

Increasing the CTA^+ concentration in the precursor mixture produces bijels with larger internal pores. The pore sizes in the center of the bijel film increase from 4 µm at 32 mM CTA^+ to 32 µm at 50 mM CTA^+, and combine into a hollow interior at 55 mM CTA^+ (**Figure 3B**; for details see SI section S4). To explain how the SNP-modification with CTA^+ influences the stabilization of the bijel pores, we examine the curvature of the *t*-BA/water interface with CLSM slices from 10 µm below the film surface. For the bijel films made with 32 and 41 mM CTA^+, round water pores are separated by a thin layer of poly(*t*-BA) (**Figure 3C-*i*, *ii***). At 50 and 55 mM CTA^+ bulky poly(*t*-BA) domains space the water pores (**Figure 3C-*iii*, *iv***). The, however, consistent curvature of poly(*t*-BA) around water indicates that the SNPs are preferentially wetted by *t*-BA.[33,34] The hydrophobic SNP wetting behavior is supported by emulsification experiments showing that the SNPs stabilize water-in-*t*-BA emulsions for phase separated precursor mixtures containing 32-55 mM CTA^+ (**Figure 3D**, Figure S4). Thus, the hydrophobization of the SNPs by CTA^+ can induce a round curvature of the *t*-BA/water interface.

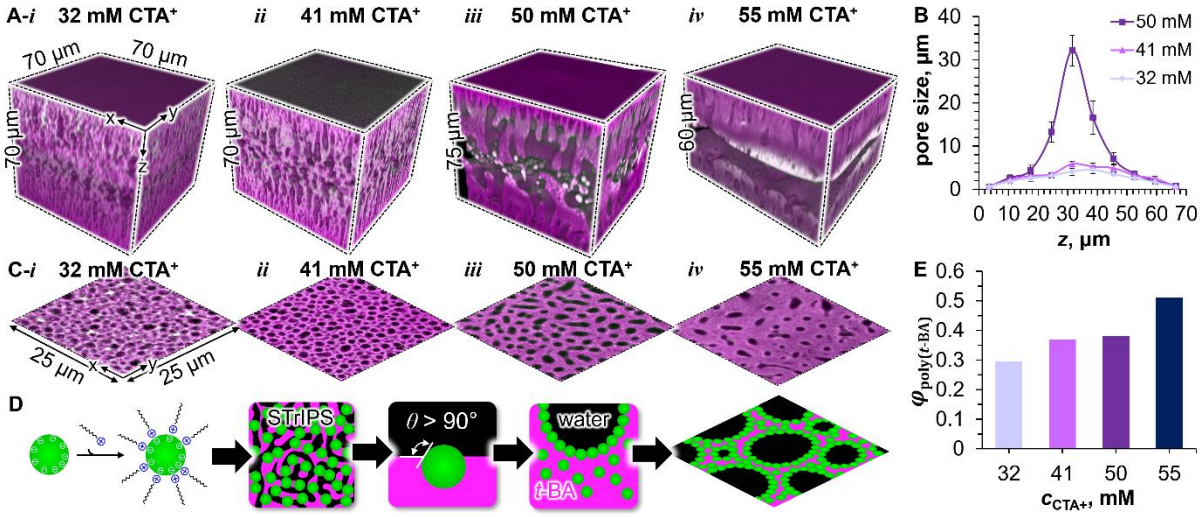

Figure 3. Effect of CTA^+ concentration on bijel film structure. **A** 3D-CSLM images of bijel films prepared with ***i*** 32 mM, ***ii*** 41 mM, ***iii*** 50 mM, and ***iv*** 55 mM CTA^+ in the precursor mixture. Magenta colour represents poly(*t*-BA), black colour water and green colour SNPs. **B** Bijel pore size plotted against film depth *z*. The line is to guide the eyes. **C** CLSM micrographs from $z = 10$ µm below the top surface. **D** CTA^+-functionalization of SNPs and effect of SNP wetting on interfacial curvature. **E** poly(*t*-BA) volume fraction $\varphi_{poly(t-BA)}$ for the bijel films presented in A.

Likewise, the CTA^+-functionalization promotes the partitioning of SNPs into the *t*-BA domains of the bijel. We measure the poly(*t*-BA) volume fraction ($\varphi_{poly(t-BA)}$) from the CLSM *z*-stacks of the bijels presented in Figure 3A. $\varphi_{poly(t-BA)}$ increases from 0.3 for the bijel film made with 32 mM CTA^+ to

0.51 at 55 mM CTA^+ (**Figure 3E**; for details see SI section S6). This trend suggests that higher CTA^+ concentrations favor the distribution of SNPs into *t*-BA, leading to an increase in $\varphi_{poly(t-BA)}$. The partitioning of the SNPs can reduce their availability to arrest the phase separation, potentially explaining the formation of bijel films with larger water pores and bulky poly(*t*-BA) domains for increasing CTA^+ concentration.[31]

To conclude, we find that adjusting the CTA^+ concentration in the precursor mixture improves the wetting of the SNP by *t*-BA and thereby, facilitates the formation of bijels with larger domains. Using this control over the porous bijel structure, we continue our study by converting the bijel film into permeable hydrogel filtration membranes. In the last section, we demonstrate the application of bijel-templated hydrogels in pH-responsive water filtration.

2.4 Hydrogel preparation and pH-responsive membrane filtration

We prepare the hydrogel membrane from hydrolyzing the polymerized bijel film made with 50 mM CTA^+ in the precursor mixture. This bijel film exhibits water pores extend from the top to the bottom surface, an important feature for creating permeable filtration membranes (**Figure 4A**). Hydrolysis of the polymerized bijel converts poly(*t*-BA) into polyacrylic acid (PAA; **Figure 4B**). The resulting PAA hydrogel membranes are kept in water of pH 5. When raising the pH of the water to 12, the deprotonation of PAA triggers the swelling of the hydrogel.[22,35]

The membrane swelling depends on the cross-linking of PAA with BDA embedded in the former poly(*t*-BA) matrix. We analyze the swelling for hydrogel membranes prepared from bijel precursors containing different BDA concentrations in the *t*-BA solution ($m_{BDA}/m_{t\text{-}BA}$ = 0.02, 0.08, 0.15, 0.25; for details see SI section S7). **Figure 4C** shows that for BDA concentrations up to $m_{BDA}/m_{t\text{-}BA}$ = 0.08 the hydrogel membranes swell by more than twice their original area. Further increasing $m_{BDA}/m_{t\text{-}BA}$ to 0.25 significantly reduces the area increase upon swelling. Cross-linking thus reduces the hydrogel swelling, but how does the swelling impact the porosity of the hydrogel membrane?

To answer this question, we visualize the hydrogel surface during swelling using CLSM and label PAA with the fluorescence dye Coumarin 6. The confocal micrographs in **Figure 4D** show that the swelling of the hydrogel made with $m_{BDA}/m_{t\text{-}BA}$ = 0.02 leads to a closure of the membrane surface pores. Likewise, hydrogel swelling also closes the surface pores of the membrane for $m_{BDA}/m_{t\text{-}BA}$ = 0.08 (**Figure 4E-*i***). In contrast, the surface pores stay open for the hydrogels swollen at $m_{BDA}/m_{t\text{-}BA}$ = 0.15 (**Figure 4E-*ii***) and 0.25 (**Figure 4E-*iii***). The CLSM analysis demonstrates that pH-induced swelling of the hydrogel enables the closure of the membrane surface pores.

The pH-regulated membrane porosity makes the hydrogels well-suited for applications in pH-sensitive water filtration. We measure the water permeability of the hydrogel membranes prepared with different BDA concentrations upon increasing the pH of the water feed from 5 to 12 (**Figure 4F**). The hydrogel made with $m_{BDA}/m_{t\text{-}BA}$ = 0.08 shows a water permeability at pH 5 of 50 L/(h*m^2*bar). For the same pH,

the water permeability increases to 69 L/(h*m^2*bar) at $m_{BDA}/m_{t\text{-}BA}$ = 0.25. The increasing water permeability with higher $m_{BDA}/m_{t\text{-}BA}$ ratios potentially results from the improved hydrogel cross-linking, making the membrane pores more resistant to deformations during filtration.[36,37]

When raising the pH of the water feed to 12, we find that the flow of water is blocked by the closed surface pores of the swollen hydrogel at $m_{BDA}/m_{t\text{-}BA}$ = 0.08. The hydrogel membranes prepared with $m_{BDA}/m_{t\text{-}BA}$ = 0.15 and $m_{BDA}/m_{t\text{-}BA}$ = 0.25 still allow for water flow at pH 12 but show a lower water permeability compared to pH 5 because swelling narrows the membrane surface pores. Membrane swelling hence controls the water permeability by pH-induced changes of the hydrogel porosity.

We show the reversibility of the swelling process by measuring the water flux for repeated cycles of membrane swelling and deswelling. To this end, hydrogel membranes prepared with $m_{BDA}/m_{t\text{-}BA}$ = 0.08 are alternately equilibrated at pH 5 and pH 12 until five consecutive cycles of hydrogel swelling and deswelling are completed (**Figure 4G-*i***, for details see SI section S8). The water flux is measured for each cycle with individual hydrogels as they are sensitive to damages during repeated assembly of the flux testing device. Therefore, we can test the restorability of pore opening and closure during continued membrane swelling/deswelling, but not the effects of repeated filtration on hydrogel permeability.

Figure 4G-*ii* shows that the water flux of the hydrogel membranes ranges between 40-50 L/(h*m^2) at pH 5 over a total of five cycles of hydrogel swelling/deswelling. Similarly, the flux consistently drops to 0 L/(h*m^2) at pH 12 across all pH-cycles. The recurrent water flux at pH 5 and the blockage of flow at pH 12 indicates that the hydrogel can reversibly close and re-open the membrane surface pores in response to changes in the solution pH.

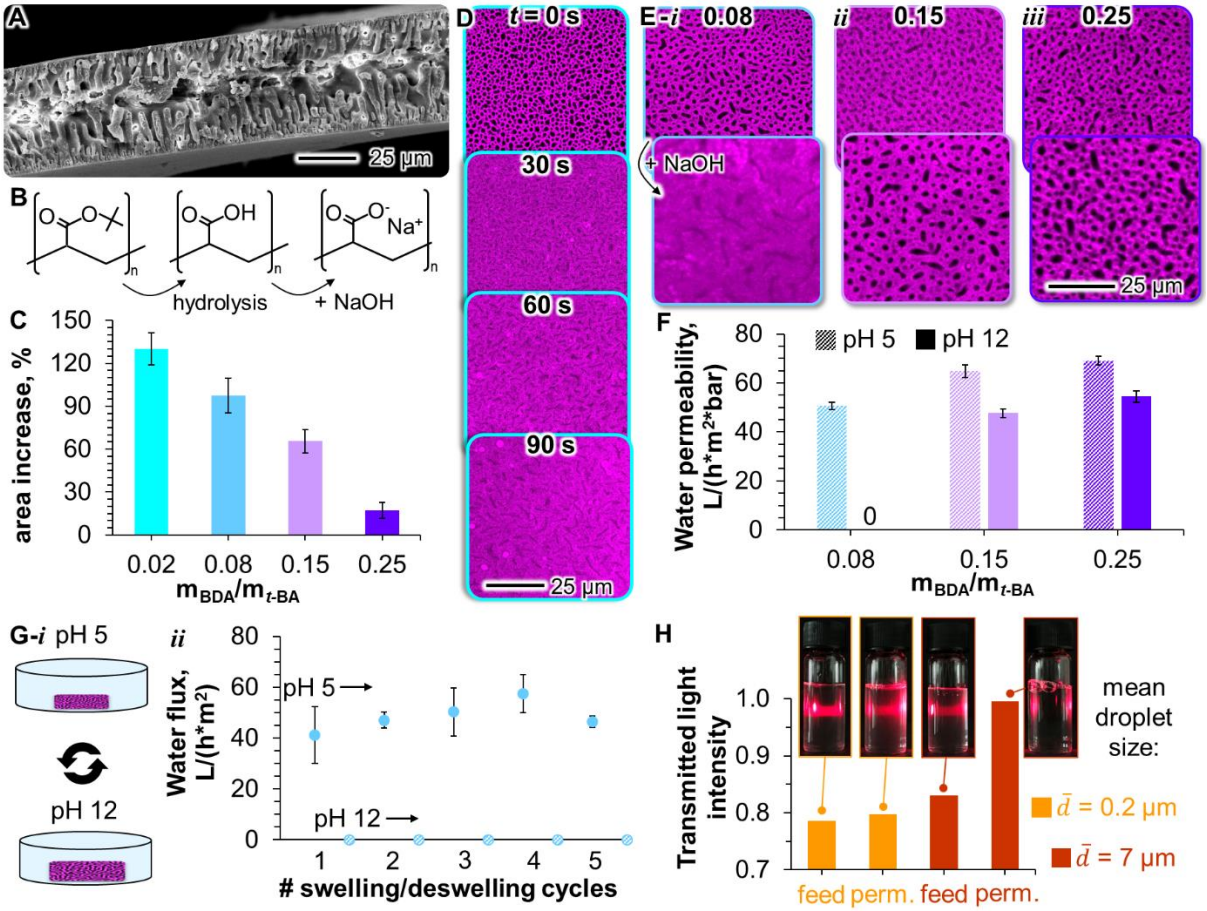

Figure 4. Swelling and pH-responsive filtrations with bijel-templated hydrogel membranes. **A** SEM image of the cross-section of the polymerized bijel film prepared with 50 mM CTA^+. **B** Hydrolysis reaction of poly(*t*-BA) to polyacrylic acid (PAA) and deprotonation of PAA by adding sodium hydroxide. **C** Percentage area change of hydrogel membranes upon swelling for different mass ratios $m_{BDA}/m_{t\text{-}BA}$ in the bijel precursor mixture. **D** CLSM images of the hydrogel surface pores (acquired at $z \approx 5$ µm) during swelling for $m_{BDA}/m_{t\text{-}BA} = 0.02$. PAA is coloured in magenta and water in black. **E-*i*, *ii*, *iii*** CLSM images of the hydrogel surface pores ($z \approx 5$ µm) upon swelling for hydrogels fabricated with different $m_{BDA}/m_{t\text{-}BA}$ ratios 0.08, 0.15, and 0.25. **F** Water permeability for hydrogel membranes made with different $m_{BDA}/m_{t\text{-}BA}$ ratios at pH 5 and pH 12 with water feed of the same pH. **G-*i*** Repeated cycles of swelling and deswelling hydrogels prepared with $m_{BDA}/m_{t\text{-}BA} = 0.08$ for ***ii*** water flux measurements at pH 5 (solid dots) and pH 12 (dashed dots) at 1 bar. **H** Separation of emulsions with mean droplet sizes $\bar{d}$ = 0.2 µm and 7 µm. Photographs of cuvettes with feed emulsion and permeate with transmitted red laser light (650 nm). Plot gives the intensity of transmitted red light for feed and permeate samples.

The pH-responsive water flux allows the hydrogels to serve as smart filtration membranes with their porous surface imparting microfiltration properties. We demonstrate the microfiltration behavior by separating oil droplets from emulsion feeds with droplets of mean sizes of 0.2 µm and 7 µm, respectively (for details see SI section S8). The emulsions are filtered separately across the hydrogel membrane (pH 5; $m_{BDA}/m_{t\text{-}BA} = 0.15$). We measure the turbidity of emulsion feed and permeate and determine the droplet separation from the difference in transmitted light intensity.

Figure 4H illustrates the turbidity measurement with red laser light shining through feed and permeate samples. The laser is visible as light beam in the emulsion feed because the oil droplets scatter the incident light. We observe the light beam also in the permeate sample obtained from filtering the 0.2 µm

oil droplets. Given the similar intensities of the transmitted laser light for both 0.2 µm emulsion feed and permeate sample, this indicates that the sub-micrometer oil droplets have passed through the hydrogel membrane. In contrast, the permeate collected from filtering the emulsion with the micron-sized oil droplets is transparent. As the corresponding transmitted light intensity increases from 0.8 for the feed to 1.0 for the permeate, we conclude that oil droplets of 7 µm average size have been separated by the hydrogel membrane (for details see SI section S9). Both the emulsion separation and flux measurements showcase the application of *bijel-templated hydrogels as microfiltration membranes with pH-responsive water permeability*.

3. Conclusions

In this study, we introduce the synthesis of bijel-templated hydrogel membranes for pH-responsive water filtration. Bijel membranes are fabricated *via* roll-2-roll solvent transfer induced phase separation (R2R-STrIPS). For R2R-STrIPS, we coat the bijel precursor mixture composed of *tertiary*-butyl acrylate (*t*-BA), 1,4-butanediol diacrylate, ethanol, water, silica nanoparticles (SNPs) and CTAB surfactant onto flat-sheet substrates. While the resulting bijel membranes adhere to hydrophobic substrate materials, we show that bijel de-wetting on hydrophilic cellulose substrate enables the collection of free-standing, polymerized bijel membranes from R2R-synthesis. To employ the bijel membranes as filtration material, we create a permeable bijel microstructure by increasing the CTAB-functionalization of the SNPs. We demonstrate that higher CTAB concentrations change the interfacial wetting behavior of the SNPs to produce bijel membranes with larger internal pores. Subsequent hydrolysis transforms these bijels into polyacrylic acid (PAA) hydrogel membranes with enhanced mechanical flexibility. The PAA hydrogels swell in response to increasing solution pH, with the extent of swelling dependent on the hydrogel cross-linker concentration. Confocal microscopy analysis reveals that low cross-linker concentrations facilitate the closure of the hydrogel surface pores during swelling. Complementary flux tests demonstrate that hydrogel swelling regulates the water permeability by alternately blocking and enabling the flow of water during recurring shifts in solution pH. Emulsion rejection experiments confirm the ability of the hydrogel membrane for microfiltration of oil droplets from an aqueous feed. The pH-responsive microfiltration hydrogels demonstrate the use of bijels as functional templates for smart filtration membranes with dynamic control over flow and selectivity, offering promising applications in filtration, drug delivery, and tissue engineering.

4. Materials and methods

4.1 Bijel precursor preparation

The bijel precursor is composed of a homogeneous liquid mixture of 27 vol-% *tertiary*-butyl acrylate (*t*-BA; Alfa Aesa), 28 vol-% water (MilliQ purification systems) and 45 vol-% ethanol (EtOH; Merck). The *t*-BA liquid contains 1 wt-% of the photo-initiator 2-hydroxy-2-methylpropiophenone (Sigma Aldrich), 8 wt-% 1,4-butanediol diacrylate (BDA; Sigma Aldrich) and the dye Nile red (Sigma Aldrich).

For variation of the cross-linker concentration, 2 wt-%, 15 wt-%, and 25 wt-% BDA are incorporated into the *t*-BA solution. The ternary phase diagrams are reported in SI section S1.

In this liquid mixture Ludox TMA® nanoparticles are incorporated (34 wt-% colloidal silica, 20 nm; Sigma Aldrich) at particle weight fractions of 25 wt-% in the EtOH volume fraction and 50 wt-% in the water volume fraction. To this end, 20 mL of the Ludox TMA® dispersion are adjusted to pH 1.7 by the addition of 1 M HCl (Acros Organics) and dialyzed in EtOH overnight. The particle weight fraction (68.5 wt-%) is determined after dialysis from measuring the mass difference before and after evaporation of liquid at 100 °C (IKA RCT heating plate). Separately, 80 mL Ludox TMA® dispersion are concentrated to 52.8 wt-% particles by the evaporation of water (Rotary evaporator, Heidolph Instruments) at 60 °C and 140 mbar. Particle aggregates are removed by centrifuging the concentrate at 3270 rcf for 10 min (Allegra X-12R; Beckman Coulter) and acidified to pH 1.7 using 1 M HCl.

Bijel precursors are prepared by dissolving 56.3 mg, 71.9 mg, 87.5 mg, and 95.3 mg cetyltrimethylammonium bromide (CTA^+) in 0.954 g of the *t*-BA solution, respectively (see Table S2). Then, 1.177 g EtOH and 0.764 g of the nanoparticle dispersion dialyzed in EtOH are added. The mixtures are placed on a heating plate for 15 min at 50 °C to facilitate dissolution of CTA^+. Last, 2.226 g of the concentrated aqueous Ludox TMA® dispersion and 0.078 g water (pH 1.7) are added followed by 30 sec ultrasonication (Branson 1800) to disperse the nanoparticles in the precursor mixtures.

4.2 Bijel film fabrication

Bijel films are synthesized *via* R2R-STrIPS.[30] The bijel precursor is pumped at 3.50 mL/min (AL-300 syringe pump; World Precision Instruments) through a glass slit coated with 0.2 wt-% PDADMAC (250-350 kDa, 500 mM NaCl; Sigma Aldrich) onto a substrate. The substrate is pulled at 5-6 cm/s through a tank filled with water of pH 1.7 and 5 vol-% EtOH. As substrates polyethylene terephthalate (PET; 100 µm thick, Reflectiv), cellulose acetate (Replicating tape, 22 µm thick, SPI Supplies) and cellulose (dialysis tubing; MWCO 14 kDa, Carl Roth) are employed.

The bijel films are polymerized by exposure to high-intensity UV-light (320-500 nm; OmniCure Series 1500) for 2 min. To fluorescently label the nanoparticles, the films are washed in a mixture of 50 vol-% 1M HCl and 50 vol-% EtOH at 50 °C and immersed in an alkaline solution of Rhodamine 110 chloride (Chemodex).[31]

4.3 Bijel film structure characterization

Confocal laser scanning micrsocopy (Stellaris 5; Leica Microsystems) is employed to analyze the bijel structure. The polymerized bijel films are immersed in Dimethyl sulfoxide (DMSO; Sigma Aldrich) to attain optical transparency (n = 1.479). The fluorescence of Rhodamine 110 chloride is excited with 488 nm laser light and detected at 500-550 nm. 561 nm laser light is used to capture the fluorescence of Nile red at 600-750 nm (Figure S2). *z*-stacks are acquired at 0.4 µm focal step size applying *z*-compensation mode due to photobleaching of Nile red.

The bijel pore sizes are measured from the confocal images obtained from Nile red fluorescence. SI section S4 describes the binarization and thresholding of the confocal images to outline the poly(*t*-BA) and water domains. The arithmetic mean of pore width and length is calculated for water pores in each 8 µm *z*-slice. The poly(*t*-BA) volume fraction is analyzed from pixel count analysis of the processed confocal micrographs as described in SI section S4. For scanning electron microscopy, the bijel films are dried and sputter-coated with 6 nm Platinum (15 kV incident electron beam; Zeiss GeminiSEM 450).

4.4 Contact angle measurements

8 µL *t*-BA is dispensed onto PET, cellulose acetate, and cellulose in water (pH 1.7). A pendant drop tensiometer (Dataphysics OCA25 with Thorlabs CS165MU/M camera) is used to measure the contact angle of the *t*-BA droplet by fitting the droplet shape (SCA20 software). The contact angle is averaged from three measurements. For analysis of the precursor wetting 8 µL of particle-free precursor mixtures containing 41 mM CTA^+ ($m_{BDA}/m_{t\text{-}BA}$ = 0.08) is injected at 2 µL/s onto the substrates in water (pH 1.7).

4.5 Bijel hydrolysis and hydrogel characterization

Hydrolysis of the bijel films is carried out in a solution of 20 wt-% formic acid (Sigma Aldrich) and 80 wt-% trifluoroacetic acid (Sigma Aldrich) for 12 h. The resulting hydrogels are washed three times each in EtOH and water, and then stored in water (pH 5). Hydrogel swelling is induced by increasing the pH of the water to 12 by the addition of 0.1 M NaOH (Merck KGaA). The membrane area increase upon swelling is calculated from measuring the change in width and length of three hydrogel pieces (Mitutoyo calliper) for BDA cross-linker concentrations of $m_{BDA}/m_{t\text{-}BA}$ = 0.02, 0.08, 0.15, and 0.25 (for details see SI section S7).

Confocal imaging of the hydrogels is performed in water of pH 5 and pH 12 (561 nm laser excitation, 600-750 nm detection range). To fluorescently label polyacrylic acid, the dye Nile red is replaced by Coumarin 6 (Sigma Aldrich) in the bijel precursor.

4.6 Hydrogel permability

The pure water permeability is measured using a home-built filtration device (for details see SI section S8). The hydrogel membranes are stored in water of pH 5 and pH 12 and placed on a Nylon microfiltration support (RS10539; Tisch Scientific). Air is expelled from the device by flushing with water for 20 min at 0.5 bar. The permeability is measured for water feeds adjusted to pH 5 and pH 12 at pressures ranging from 0.25 to 1.5 bar. After equilibrating the membrane for 2 min at each pressure, permeate samples are collected for 2 min and the permeability is calculated from the retrieved mass of water.

To measure the water flux upon repetitive cycles of membrane swelling and deswelling, the hydrogels are consecutiveley immersed in water of pH 5 and pH 12 for 30 min each. Individual hydrogel membranes are subjected to these pH cycles until the required number of cycles is reached. For each cycle, the water flux is measured from three hydrogels at a pressure of 1 bar. Permeate samples are

collected for 2 min from the hydrogels tested at pH 5 while permeate sampling is performed for 30 min for the hydrogels at pH 12.

4.7 Emulsion separation

Emulsions are prepared by dissolving 0.2 mM Triton X-100 (Sigma Aldrich) in 98 g water (MilliQ) followed by the addition of 2 g light mineral oil (mixture of liquid hydrocarbons; Sigma Aldrich). Mineral oil is emulsified *via* tip-sonication at 50 % amplitude for 1 min (500 W tip sonicator, 10 mm tip diameter; Qsonica LCC) under continuous stirring at 150 rpm (IKA color squid). The droplet sizes are measured using dynamic light scattering (Zetasizer Ultra, Malvern Panalytical) after diluting the emulsion 1:100 in pure water. The emulsion stability is characterized from measuring droplet size and Zeta-potential 1 h, 2 h, and 8 h after emulsification. A second emulsion batch is prepared by stirring of 2 g mineral oil for 1 h at 450 rpm in 98 g water containing 0.2 mM Triton X-100. The oil droplet sizes are measured from brightfield microscopy images taken directly after emulsification and 1 h, 2 h, and 8 h later (for details see SI section S9).

The emulsion separation is tested for dilute emulsions at pH 5 (dilution in water; 1:100 for tip-sonicated emulsion, 1:10 for stirred emulsion) using a home-built dead-end filtration device. The emulsion feed is stirred at 200 rpm, and the droplet separation is tested for three hydrogel membranes (made with 50 mM CTA^+, $m_{BDA}/m_{t\text{-}BA} = 0.15$; 200 µm wire cloth support, Franz Eckert GmbH) by collecting permeate samples for 30 min at 0.75 bar. Droplet rejection is analyzed by measuring the intensity of UV-Vis light transmitted through feed and permeate samples using a spectrophotometer (Lambda 365+, Perkin Elmer; 200-1100 nm wavelength range, 1 nm scan interval; Quartz cuvettes, Hellma; type 110-QS). After baseline correction for pure water, the intensity of transmitted light I_{trans} is calculated from the measured absorbance I_{abs} as $I_{trans} = 1 - I_{abs}$ with $I_{trans} = 1$ referring to the transmitted intensity for pure water.

Notes

The authors declare no competing financial interest.

Author information

Corresponding author

M. F. Haase - Van't Hoff Laboratory of Physical and Colloid Chemistry, Department of Chemistry, Debye Institute for Nanomaterials Science, Utrecht University, Utrecht, The Netherlands; Email: m.f.haase@uu.nl

Authors

H. Siegel - Van't Hoff Laboratory of Physical and Colloid Chemistry, Department of Chemistry, Debye Institute for Nanomaterials Science, Utrecht University, Utrecht, The Netherlands

Acknowledgement

This publication is part of the project "Bijel templated membranes for molecular separations" (with project number 18632 of the research program Vidi 2019) which is financed by the Dutch Research Council (NWO). We thank Erik Betz-Güttner for kind support in scanning electron microscopy.

Declaration of generative AI and AI-assisted technologies in the writing process

During the preparation of this work the authors used ChatGPT in order to improve the sentence structure and grammar of the main text. After using this tool/service, the authors reviewed and edited the content as needed and take full responsibility for the content of the publication.

References

1. Yin, J. & Deng, B. Polymer-matrix nanocomposite membranes for water treatment. *J. Memb. Sci.* **479**, 256–275 (2015).
2. Charcosset, C. Classical and Recent Applications of Membrane Processes in the Food Industry. *Food Eng. Rev.* **13**, 322–343 (2021).
3. Karki, S., Hazarika, G., Yadav, D. & Ingole, P. G. Polymeric membranes for industrial applications: Recent progress, challenges and perspectives. *Desalination* **573**, 117200 (2024).
4. Prykhodko, Y., Fatyeyeva, K., Hespel, L. & Marais, S. Progress in hybrid composite Nafion®-based membranes for proton exchange fuel cell application. *Chem. Eng. J.* **409**, 127329 (2021).
5. Sidhikku Kandath Valappil, R., Ghasem, N. & Al-Marzouqi, M. Current and future trends in polymer membrane-based gas separation technology: A comprehensive review. *J. Ind. Eng. Chem.* **98**, 103–129 (2021).
6. Huang, T. *et al.* Advanced stimuli-responsive membranes for smart separation. *Chem. Soc. Rev.* **52**, 4173–4207 (2023).
7. Wandera, D., Wickramasinghe, S. R. & Husson, S. M. Stimuli-responsive membranes. *J. Memb. Sci.* **357**, 6–35 (2010).
8. Zou, L.-B. *et al.* Smart membranes for biomedical applications. *Chinese J. Chem. Eng.* **49**, 34–45 (2022).
9. Yang, Z. *et al.* A Critical Review on Thin-Film Nanocomposite Membranes with Interlayered Structure: Mechanisms, Recent Developments, and Environmental Applications. *Environ. Sci. Technol.* **54**, 15563–15583 (2020).
10. Zhao, C., Nie, S., Tang, M. & Sun, S. Polymeric pH-sensitive membranes—A review. *Prog. Polym. Sci.* **36**, 1499–1520 (2011).

11. Mah, E. & Ghosh, R. Thermo-Responsive Hydrogels for Stimuli-Responsive Membranes. *Processes* **1**, 238–262 (2013).

12. Pantuso, E., De Filpo, G. & Nicoletta, F. P. Light-Responsive Polymer Membranes. *Adv. Opt. Mater.* **7**, (2019).

13. Liu, H. *et al.* Thermo- and pH-responsive graphene oxide membranes with tunable nanochannels for water gating and permeability of small molecules. *J. Memb. Sci.* **587**, 117163 (2019).

14. Li, P.-F. *et al.* Regulation of Critical Ethanol Response Concentrations of Ethanol-Responsive Smart Gating Membranes. *Ind. Eng. Chem. Res.* **51**, 9554–9563 (2012).

15. Wang, Y. *et al.* A novel smart membrane with ion-recognizable nanogels as gates on interconnected pores for simple and rapid detection of trace lead(II) ions in water. *J. Memb. Sci.* **575**, 28–37 (2019).

16. Dirksen, M. *et al.* UV cross-linked smart microgel membranes as free-standing diffusion barriers and nanoparticle bearing catalytic films. *RSC Adv.* **11**, 22014–22024 (2021).

17. Tokarev, I. & Minko, S. Stimuli-Responsive Porous Hydrogels at Interfaces for Molecular Filtration, Separation, Controlled Release, and Gating in Capsules and Membranes. *Adv. Mater.* **22**, 3446–3462 (2010).

18. Lin, Y. *et al.* Surface modification of PVA hydrogel membranes with carboxybetaine methacrylate via PET-RAFT for anti-fouling. *Polymer (Guildf).* **162**, 80–90 (2019).

19. Chang, H. *et al.* State-of-the-art insights on applications of hydrogel membranes in water and wastewater treatment. *Sep. Purif. Technol.* **308**, 122948 (2023).

20. Yazdi, M. K. *et al.* Hydrogel membranes: A review. *Mater. Sci. Eng. C* **114**, 111023 (2020).

21. Thoniyot, P., Tan, M. J., Karim, A. A., Young, D. J. & Loh, X. J. Nanoparticle–Hydrogel Composites: Concept, Design, and Applications of These Promising, Multi-Functional Materials. *Adv. Sci.* **2**, (2015).

22. Kharal, S. P. & Haase, M. F. Centrifugal Assembly of Helical Bijel Fibers for pH Responsive Composite Hydrogels. *Small* **18**, (2022).

23. Haase, M. F. *et al.* Multifunctional nanocomposite hollow fiber membranes by solvent transfer induced phase separation. *Nat. Commun. 2017* **8**, 1–7 (2017).

24. Thorson, T. J., Botvinick, E. L. & Mohraz, A. Composite Bijel-Templated Hydrogels for Cell Delivery. *ACS Biomater. Sci. Eng.* **4**, 587–594 (2018).

25. Thorson, T. J., Gurlin, R. E., Botvinick, E. L. & Mohraz, A. Bijel-templated implantable biomaterials for enhancing tissue integration and vascularization. *Acta Biomater.* **94**, 173–182 (2019).

26. Pizzetti, F., Massobrio, G., Riva, S., Vangosa, F. B. & Rossi, F. Biphasic Porous Bijel-Like Structures with Hydrogel Domains as Controlled Drug Delivery Systems. *Gels* **10**, 72 (2024).

27. Haase, M. F., Stebe, K. J. & Lee, D. Continuous Fabrication of Hierarchical and Asymmetric Bijel Microparticles, Fibers, and Membranes by Solvent Transfer-Induced Phase Separation (STRIPS). *Adv. Mater.* **27**, 7065–7071 (2015).

28. Herzig, E. M., White, K. A., Schofield, A. B., Poon, W. C. K. & Clegg, P. S. Bicontinuous emulsions stabilized solely by colloidal particles. *Nat. Mater. 2007 612* **6**, 966–971 (2007).

29. Yang, Q., Adrus, N., Tomicki, F. & Ulbricht, M. Composites of functional polymeric hydrogels and porous membranes. *J. Mater. Chem.* **21**, 2783–2811 (2011).

30. Siegel, H., de Ruiter, M., Athanasiou, G., Hesseling, C. M. & Haase, M. F. Roll-to-Roll Fabrication of Bijels via Solvent Transfer Induced Phase Separation (R2R-STrIPS). *Adv. Mater. Technol.* **9**, 2301525 (2024).

31. Siegel, H. *et al.* Synthesis and Polyelectrolyte Functionalization of Hollow Fiber Membranes Formed by Solvent Transfer Induced Phase Separation. *ACS Appl. Mater. Interfaces* **14**, 43195–43206 (2022).

32. Sprockel, A. J. *et al.* Fabrication of bijels with sub-micron domains via a single-channel flow device. *Colloids Surfaces A Physicochem. Eng. Asp.* **666**, 131306 (2023).

33. Binks, B. P., Rodrigues, J. A. & Frith, W. J. Synergistic interaction in emulsions stabilized by a mixture of silica nanoparticles and cationic surfactant. *Langmuir* **23**, 3626–3636 (2007).

34. Cui, Z. G., Yang, L. L., Cui, Y. Z. & Binks, B. P. Effects of Surfactant Structure on the Phase Inversion of Emulsions Stabilized by Mixtures of Silica Nanoparticles and Cationic Surfactant. *Langmuir* **26**, 4717–4724 (2009).

35. Dickhaus, B. N. & Priefer, R. Determination of polyelectrolyte pKa values using surface-to-air tension measurements. *Colloids Surfaces A Physicochem. Eng. Asp.* **488**, 15–19 (2016).

36. Kallioinen, M., Pekkarinen, M., Mänttäri, M., Nuortila-Jokinen, J. & Nyström, M. Comparison of the performance of two different regenerated cellulose ultrafiltration membranes at high filtration pressure. *J. Memb. Sci.* **294**, 93–102 (2007).

37. Persson, K. M., Gekas, V. & Trägardh, G. Study of membrane compaction and its influence on ultrafiltration water permeability. *J. Memb. Sci.* **100**, 155–162 (1995).